# NJC

Accepted Manuscript


This is an *Accepted Manuscript*, which has been through the Royal Society of Chemistry peer review process and has been accepted for publication.

*Accepted Manuscripts* are published online shortly after acceptance, before technical editing, formatting and proof reading. Using this free service, authors can make their results available to the community, in citable form, before we publish the edited article. We will replace this *Accepted Manuscript* with the edited and formatted *Advance Article* as soon as it is available.

You can find more information about *Accepted Manuscripts* in the Information for Authors.

Please note that technical editing may introduce minor changes to the text and/or graphics, which may alter content. The journal's standard Terms & Conditions and the Ethical guidelines still apply. In no event shall the Royal Society of Chemistry be held responsible for any errors or omissions in this *Accepted Manuscript* or any consequences arising from the use of any information it contains.

ROYAL SOCIETY OF CHEMISTRY

www.rsc.org/njc

# Photocurrent enhancement in $Cu_2Cd(SSe)_2$ photoanode synthesized via arrested precipitation route

**Kishorkumar V. Khot**[a], Sawanta S. Mali[b], Vishvanath B. Ghanwat[a], Suvarta D. Kharade[a], Rahul M. Mane[a], Chang Kook Hong[b], and Popatrao N. Bhosale[a*]

[a]*Materials Research Laboratory, Department of Chemistry, Shivaji University, Kolhapur-416004, India.*

[b]*Polymer Energy Materials Laboratory, Advanced Chemical Engineering Department, Chonnam National University, Gwangju, South Korea.*

[c]*Thin film Materials Laboratory, Department of Physics, Shivaji University, Kolhapur, India.*

*Corresponding Author E-mail address: p_n_bhosale@rediffmail.com*

*khotkishor75@gmail.com, Tel Number: 091-231-2609338.*

**Abstract**

In the present investigation, nanostructured combinatorial quaternary $Cu_2Cd(SSe)_2$ thin films have been successfully synthesized *via* a self organized arrested precipitation technique (APT). The synthesized quaternary $Cu_2Cd(SSe)_2$ thin films show enhancement in photocurrent for Cu-poor composition, which signifies that the synthesized quaternary material is commensurate with other Cu-based quaternary and multinary materials for solar cell application. The optostructural study clearly illustrates that synthesized thin films have optimistic band gap energy with mixed crystal structures. The morphological study indicates that the formation of hierarchical microstructures. Compositional study confirms that the formation of quaternary thin films with mandatory composition. *J-V* curves demonstrates that photocurrent enhancement is observed in quaternary $Cu_2Cd(SSe)_2$ thin films with an increase in Cu-content. Resultant maximum short circuit current density ($J_{sc}$) and that of the open circuit voltage ($V_{oc}$) are 1.23 mA/cm$^2$ and 437 mV respectively.

***Keywords:*** *Nanostructured quaternary thin films, new hybrid chemical technique, FESEM, HRTEM, XPS, photoelectrochemical application.*

New Journal of Chemistry Accepted Manuscript

## 1 Introduction

Quite large global energy utilization and environmental concern, the development of innovative, high efficiency and low cost solar cell devices has drawn passionate researchers attention in recent years [1]. The ternary and quaternary based compounds occupy a crucial role in research of novel materials with better optostructural and optoelectronic properties [2-4]. In recent years, nanostructured semiconductor materials have attracted massive steadily growing interest in various applications. Such nanostructured materials have unique properties and different applications in the construction of various devices. Each of specific materials has special properties and limitations. So as to develop a new multifunctional system, it is crucial to incorporate various exclusive nanomaterials in a sequential manner [5]. The metal chalcogenides materials have been studied widely due to the favorable band gaps of chalcogenides unlike oxide materials, which cover a maximum visible region of the solar spectrum. However, several chalcogenide reports are available in literature survey based on quaternary thin films due to its improved chemical properties and huge capability of light absorption. Therefore, many research groups are quite engaged in the fabrication of new quaternary materials for different applications [6].

As an alternative energy source, solar energy is a potential energy source for solving the scarcity of available energy sources. Solar power is the world's most profuse and never-ending resource of energy. Hence, a year's worth of sunlight provides more than a hundred times the energy of the world's available fossil fuel reserves. Therefore, photoelectrochemical cells have gained much attention as a renewable energy source of electricity [7]. Right now, world facing problem with the critical synthesis process and the overall high production cost of solar cell devices. Therefore, it is crucial to develop new materials with superior properties demonstrates high conversion efficiency.

Considering above facts of energy crises and properties of quaternary material many scientists made great efforts on synthesis of copper zinc tin sulfide (CZTS), copper zinc tin sulfoselenide (CZTSSe) thin films in field for solar cell applications [8]. The main features of this material are cost effective, earth abundant and less toxic elements such as Cu, Zn, etc [9]. Also, CZTS thin films show the direct band gap energy of approximately at 1.5 eV, as a result, it has a high absorption coefficient of about $10^4$ $cm^{-1}$. In addition to this, copper indium gallium selenide (CIGS) thin films reached highest conversion efficiency for Cu-poor composition in the lab as well as industrial



New Journal of Chemistry Accepted Manuscript

production. Taking into account this view several researchers have spent their time to develop efficient CZTS and CIGS thin film solar cells. Overall literature survey demonstrated that the best performance of the CZTS and CIGS based solar cell is obtained through Cu-poor composition. It is well known that Cu-poor thin films are of *n*-type semiconductors [10, 11]. Also, Cu-rich chalcopyrite solar cells experience the problem of interface recombination unlike the Cu-poor [12, 13].

Nowadays, the $II^{B}$-$VI^{A}$ group chalcogenides based ternary and quaternary thin films have attracted great significance because of their unique properties and promising applications such as, photoelectrochemical (PEC) solar cell [14], optoelectronic devices [15] and light emitting diodes [16] etc. The $Cd(S_{0.2}Se_{0.8})$ thin film shows considerably improved PEC performance. Observed conversion efficiency is quite promising compared with other reported results. It indicates that the material has huge potential for improvement in PEC performance. Moreover, we have tried to construct a new pathway for development of unique quaternary based thin films for PEC application.

CdSe and CdS are very important semiconductor materials and pseudo binary compounds of Cd(SSe) thin films can be effectively used as good candidates for the solar cell applications. Cd(SSe) thin films were synthesized by various techniques such as chemical bath deposition (CBD) [17-19], sputtering [20] and evaporation techniques [21-24] etc. Among these synthesis techniques APT has achieved remarkable potential features and cost effective compared to routine aqueous chemical techniques [12, 16]. APT is self organized, cost effective technique, and suitable for large area deposition. In addition, APT is a hybrid chemical method of the chemical bath deposition (CBD) technique in combination with the controlled chemical growth process (CCGP) and prospective for synthesis of mixed metal chalcogenide (MMC) thin films at low cost manner [12, 16].

Taking into consideration key aspects of the $II^{B}$-$VI^{A}$ group ternary, quaternary chalcogenide thin films, we have constructed new quaternary mixed metal chalogenide (QMMC) ($Cu_2Cd(S_{0.2}Se_{0.8})_2$) thin films. In the present investigation, the main aim is to study the effect of copper content in Cd(SSe) and develop the new photoactive QMMC thin films through chemical process. Finally deposited QMMC thin films were tested for its PEC application. As well reaction, possible growth mechanism of QMMC thin film formation via APT and redox reaction mechanism in the PEC cell was discussed in detail with schematic representation.



New Journal of Chemistry Accepted Manuscript

## 2 Experimental details

### 2.1 Chemicals

All chemicals were of analytical reagent (AR) grade and used without further purification. Cupric sulfate pentahydrate ($CuSO_4 \cdot 5H_2O$) (99.5 %, s d fine-chem.), cadmium sulfate monohydrate ($CdSO_4 \cdot H_2O$) (98 %, s d fine-chem.), thiourea ($H_2N\text{-}CS\text{-}NH_2$) (99 %, s d fine-chem.) selenium metal powder (99.5 %, Sigma Aldrich), anhydrous sodium sulfite ($Na_2SO_3$) (96 %, s d fine-chem.), liquor ammonia ($NH_3$) (28-30 % Thomas Baker), and triethanolamine ($N(CH_2\text{-}CH_2\text{-}OH)_3$) (99 %, Merck) were used as precursors and complexing agent respectively. For measurement of PEC cell properties we have used sulfide/polysulfide redox electrolyte prepared from sodium sulfide ($Na_2S$) (55-58 %, Thomas Baker), sodium hydroxide pellets (NaOH) (99 %, s d fine-chem.) and sulfur powder (99 %, s d fine-chem.). Herein, $Cu_2Cd(SSe)_2$ thin films were deposited onto bare as well as ITO (Indium Doped Tin Oxide) coated glass substrates (sheet resistance 20-25 $\Omega\ cm^{-2}$) by using simple APT.

**Preparation of solutions**

$Cu_2Cd(SSe)_2$ thin films were synthesized on ultrasonically cleaned glass and ITO coated glass substrate by APT. All the precursor solutions were prepared in double distilled water and solution preparation procedure is given as follows,

**Copper-triethanolamine (Cu-TEA) complex**

0.1 M Cu-TEA complex was prepared by triturating 2.49 g $CuSO_4 \cdot 5H_2O$ with TEA and diluted to 100 mL with double distilled water.

**Cadmium-triethanolamine (Cd-TEA) complex**

0.05 M Cd-TEA complex was prepared by triturating 1.28 g $CdSO_4 \cdot H_2O$ with TEA and diluted to 100 mL with double distilled water.

**Thiourea**

0.05 M $H_2N\text{-}CS\text{-}NH_2$ solution was prepared by dissolving 0.38 g of $H_2N\text{-}CS\text{-}NH_2$ in double distilled water and diluted to 100 mL with distilled water.

**Sodium selenosulfite**

0.25 M $Na_2SeSO_3$ solution was prepared by refluxing 6 g of selenium metal powder (Se) and 30 g anhydrous $Na_2SO_3$ in 250 mL distilled water at 90°C for 8 h in a 500 ml round bottom flask. 0.05 M $Na_2SeSO_3$ solution was used as $Se^{2-}$ source, which prepared by diluting 0.25 M $Na_2SeSO_3$ solution using double distilled water.



New Journal of Chemistry Accepted Manuscript

### 2.2 Synthesis of $Cu_2Cd(SSe)_2$ thin films

In our synthesis method, metal ions were arrested using a suitable complexing agent and thin film formation occurs through slow ion by ion condensation of ions *via* multinucleation process. In actual deposition, Cu-TEA, Cd-TEA complex react with $S^{2-}$ and $Se^{2-}$ ions, which are slowly released from dissociation of $H_2N\text{-}CS\text{-}NH_2$ and $Na_2SeSO_3$ at alkaline pH 10.4±0.2 and 50°C±2 temperature. Excessive concentration of $Na_2SO_3$ over selenium prevents oxidation of selenide and its reprecipitation as selenium [25]. In the typical bath preparation, appropriate volume of 0.1 M Cu-TEA, 0.05 M Cd-TEA complexes were taken in 100 mL beaker with constant stirring for 5 min. Such mixture of both cations was light blue coloured, which was stabilized at pH 10.4±0.2 by drop wise addition of $NH_3$. During drop wise addition of $NH_3$ in above solution light blue coloured solution turn into dark blue. Followed this with constant stirring appropriate volume of $H_2N\text{-}CS\text{-}NH_2$ and $Na_2SeSO_3$ solutions was poured into pH stabilized reaction mixture. Furthermore, mixing of anionic precursors causes to the formation of more intense dark coloured solution. After complete preparation of reaction bath whole solution was stirred for 5 min. to form homogeneous mixture of solution and colour gets converted into light blue. Precleaned glass substrates were immersed in reaction bath using a substrate holder at an optimized reaction temperature (50°C±2) and substrate rotation 45±5 rpm for 2.3 h deposition time. After 15 minutes of reaction, light blue coloured reaction mixture became colourless. It means that excess concentration of $Na_2SO_3$ over selenium reduces $Cu^{2+}$ (II) into $Cu^{+}$ (I) ions. Further increase in deposition time $Cu^{+}$, $Cd^{2+}$ metal ions release slowly (from Cu-TEA, Cd-TEA metal complex) and reacts with $S^{2-}$, $Se^{2-}$ chalcogen ions (released from dissociation of $H_2N\text{-}CS\text{-}NH_2$ and $Na_2SeSO_3$). Followed this formation of orange-brown to blackish brown coloured (with increased Cu content) to the solution and deposition of well adherent, pinhole free and homogeneous thin film was observed. Photographs of all synthesized thin films as a function of Cu content are shown in Fig. 1.

New Journal of Chemistry Accepted Manuscript

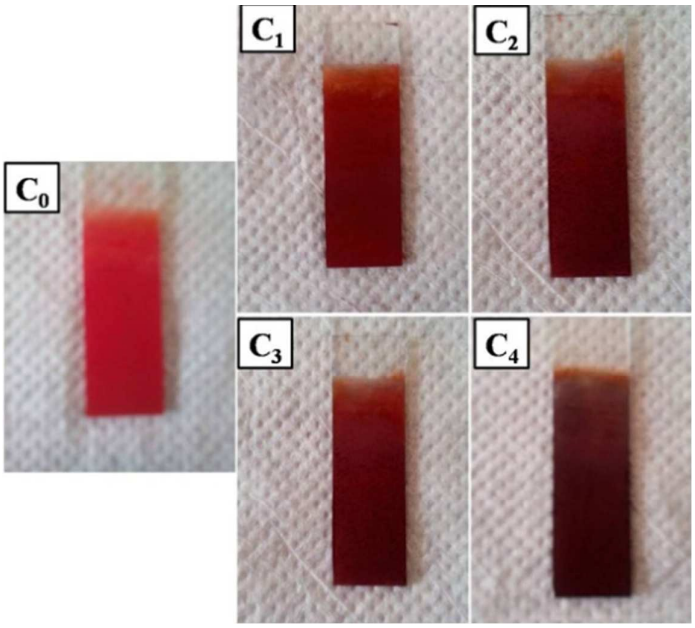


***Fig. 1*** *Photographs of synthesized $Cu_2Cd(SSe)_2$ thin films at 50°C±2 temperature for 2.30 h deposition time.*

The release of metal and chalcogen ions with colour variation in a reaction mixture denotes the formation of multinucleation centers on the substrate surface with increased in deposition time. Following this at a specific deposition time (2.30 h) formation of adherent, thicker $Cu_2Cd(SSe)_2$ thin films was occurred. Deposited thin films were washed with double distilled water, dried at room temperature and used for further characterizations. In order to study the effect of copper content on different properties and synthesis of photoactive $Cu_2Cd(SSe)_2$ QMMC thin films, Copper content in reaction mixture was varied from 0.0 mL, 0.5 mL, 1.0 mL, 1.5 mL and 2.0 mL of 0.1 M Cu-TEA complex solution and abbreviated as $C_0$, $C_1$, $C_2$, $C_3$ and $C_4$ (Table1). Actually, we have varied lower volume of Cu-content in QMMC thin films, because as per our knowledge and literature survey, low Cu content thin film shows enhanced properties and effective power conversion efficiency [26]. Also, low Cu content illustrates the formation of well adherent, pinhole free thin films [26]. In fact, we have tried to increase Cu content more than optimized volume results in formation of precipitation rather than proper desired thin film formation. The overall study concludes that the optimized Cu content shows the formation of desired thin films with improved properties. Hence, we have preferred to develop such a promising and challenging quaternary material to study their various properties for the PEC cell application.



New Journal of Chemistry Accepted Manuscript

***Table 1*** *Optimized preparative parameters of synthesized $Cu_2Cd(SSe)_2$ thin films.*

| Sample Code | Bath composition | pH | Temperature (°C) | Substrate rotation (rpm*) | Deposition time (h) |
|---|---|---|---|---|---|
| $C_0$ | 0.1 M x mL Cu-TEA + 20-x mL Cd-TEA + 0.05 M 4.0 mL $H_2N$-CS-$NH_2$ + 0.05 M 16 mL $Na_2SeSO_3$ (x= 0.0, 0.5, 1.0, 1.5 and 2.0 mL) | 10.4±0.2 | 50±2 | 45±5 | 2.30 |
| $C_1$ | | | | | |
| $C_2$ | | | | | |
| $C_3$ | | | | | |
| $C_4$ | | | | | |

### 2.3 Characterization of $Cu_2Cd(SSe)_2$ thin films

The thickness of CdS thin films was determined by using surface profiler [AMBIOS XP-1]. The optical absorption study was carried out using UV-Vis-NIR spectrophotometer [Shimadzu, UV-1800]. The structural properties were studied by using X-ray diffractometer (XRD) [Bruker AXS, D8] using Cu Kα (λ =1.5418 Å) radiation. The surface morphology and elemental composition of the CdS thin films were carried out by field emission scanning electron microscopy (FESEM) equipped with energy dispersive X-ray spectroscopy (EDS) analyzer [JEOL, JSM-6360A]. Insight morphology of the material was carried out by using high resolution transmission electron microscopy (HRTEM, TECNAI F20 Philips operated at 200 kV) and selected area electron diffraction (SAED). The elemental composition was also analyzed by using an X-ray photoelectron spectrometer (XPS, Thermo Scientific, Multilab-2000) with a multi-channel detector, which can endure high photon energies from 0.1 eV to 3.0 KeV. Electrical conductivity (EC) was measured by using two point probe method. Thermoelectric power (TEP) measurements were conducted under conditions of maximum temperature difference and minimum contact resistance. PEC performance was carried out using a semiconductor parameter analyzer (Keithley SCS-4200 Semiconductor) characterization unit in dark and under illumination using 500 W tungsten filament lamp (Intensity of 30 mW/cm$^2$) in sulfide/polysulfide redox electrolyte. PEC cell was fabricated using standard two-electrode configuration, comprising glass-



New Journal of Chemistry Accepted Manuscript

ITO/$Cu_2Cd(SSe)_2$ (active surface area 1 $cm^2$) photoelectrode, and graphite rod used as counter electrode.

## 3 Results and discussion

### 3.1 Growth and reaction mechanism of $Cu_2Cd(SSe)_2$ thin films

The possible reaction mechanism of $Cu_2Cd(SSe)_2$ thin films is as follows,

Initially, $Cu^{2+}$, $Cd^{2+}$ metal ions are released from bound metal complex of Cu-TEA, Cd-TEA as follows (reactions (1) and (2)),

$$2\,(NH_4)_4\,[Cu\ 2N(CH_2\text{-}CH_2\text{-}O)_3] + 12H_2O \xrightarrow{10.4\pm0.2} 2Cu^{2+} + 4[N(CH_2\text{-}CH_2\text{-}OH)_3] + 8NH_4OH + 4OH^- \quad (1)$$

$$(NH_4)_4\,[Cd\ 2N\ (CH_2\text{-}CH_2\text{-}O)_3] + 6H_2O \xrightarrow{10.4\pm0.2} Cd^{2+} + 2[N(CH_2\text{-}CH_2\text{-}OH)_3] + 4NH_4OH + 2OH^- \quad (2)$$

Further, at the alkaline pH, $H_2N\text{-}CS\text{-}NH_2$dissociates to release $S^{2-}$ ions, as shown in reaction (3),

$$H_2N\text{-}\overset{\overset{S}{\|}}{C}\text{-}NH_2 + OH^- \xrightarrow{10.4\pm0.2} HS^- + H_2N\text{-}\overset{\overset{O}{\|}}{C}\text{-}NH_2$$

$$HS^- + OH^- \longrightarrow S^{2-} + H_2O \quad (3)$$

Simultaneously, $Na_2SeSO_3$ dissociate into $Na_2SO_4$ and active $HSe^-$ species. These active species immediately converted into $Se^{2-}$ ions (reaction (4)) as follows,

$$Na_2SeSO_3 + OH^- \xrightarrow{10.4\pm0.2} HSe^- + Na_2SO_4$$

$$HSe^- + OH^- \longrightarrow Se^{2-} + H_2O \quad (4)$$

The excess content of $Na_2SO_3$ oxidizes into $Na_2SO_4$ and releases electrons, which are responsible for the reduction of Cu (II) into Cu (I) states, and which was confirmed by observing changes in colour of solution from blue to colourless after addition of $Na_2SeSO_3$ (equation (5)),



New Journal of Chemistry Accepted Manuscript

$$Cu^{2+} + e^{-} \longrightarrow Cu^{1+} \quad (5)$$

When the ionic product exceeds the solubility product in the reaction solution formation of thin films occurred. The overall reaction of $Cu_2Cd(SSe)_2$ thin films is as follows (reaction (6)),

$$\begin{aligned} &2\,(NH_4)_4\,[Cu\ 2N(CH_2\text{-}CH_2\text{-}O)_3] \quad + (NH_4)_4\,[Cd\ 2N\,(CH_2\text{-}CH_2\text{-}O)_3] \\ &\quad + H_2N\text{-}\overset{\overset{S}{\|}}{C}\text{-}NH_2 \quad + Na_2SeSO_3 \quad + 16H_2O \\ &\qquad\qquad \xrightarrow{10.4\pm0.2} \\ &Cu_2Cd(SSe)_2 \quad + 6[N(CH_2\text{-}CH_2\text{-}OH)_3] \quad + 12NH_4OH \quad + H_2N\text{-}\overset{\overset{O}{\|}}{C}\text{-}NH_2 \quad + Na_2SO_4 \quad + 2OH^- \end{aligned} \quad (6)$$

In APT, thin film formation occurs on the basis of Ostwald's ripening law. Ostwald's ripening process is nothing but growing big crystals at the expense of little crystals. A large number of small crystals form in a system at a preliminary stage, but disappears excluding few of that grown larger. Such smaller crystals proceed as a nucleation center for bigger one. As the large crystals grow, the area around them is depleted by the smaller crystal. Generally, a nucleation process occurs through the formation of smaller clusters of larger number of atoms in the solution phase reaction [27]. Once the nucleation proceeds formation of bigger particles is occurring through a large number of smaller one.

In the present investigation, it has been observed that formation of QMMC thin films occurred on the basis of slow release of ions from the dissociation of the complexes. In the typical reaction bath, initially metal ions ($Cu^{+}$, $Cd^{2+}$) and chalcogen ions ($S^{2-}$, $Se^{2-}$) diffuses and start to nucleate on the substrate surface continuously. Followed this initiative stage of reaction all ions start condenses rapidly at optimized reaction parameters with increase in reaction time. So, desired thin film formation observed through slow ion-by-ion condensation via multinucleation of subsequent ions on the substrate surface. First 15 min of the reaction time solution indicates the colourless solution, which indicates that nucleation does not occur. It means that, initial time is the induction phase of formation of nucleation centers [25].

New Journal of Chemistry Accepted Manuscript

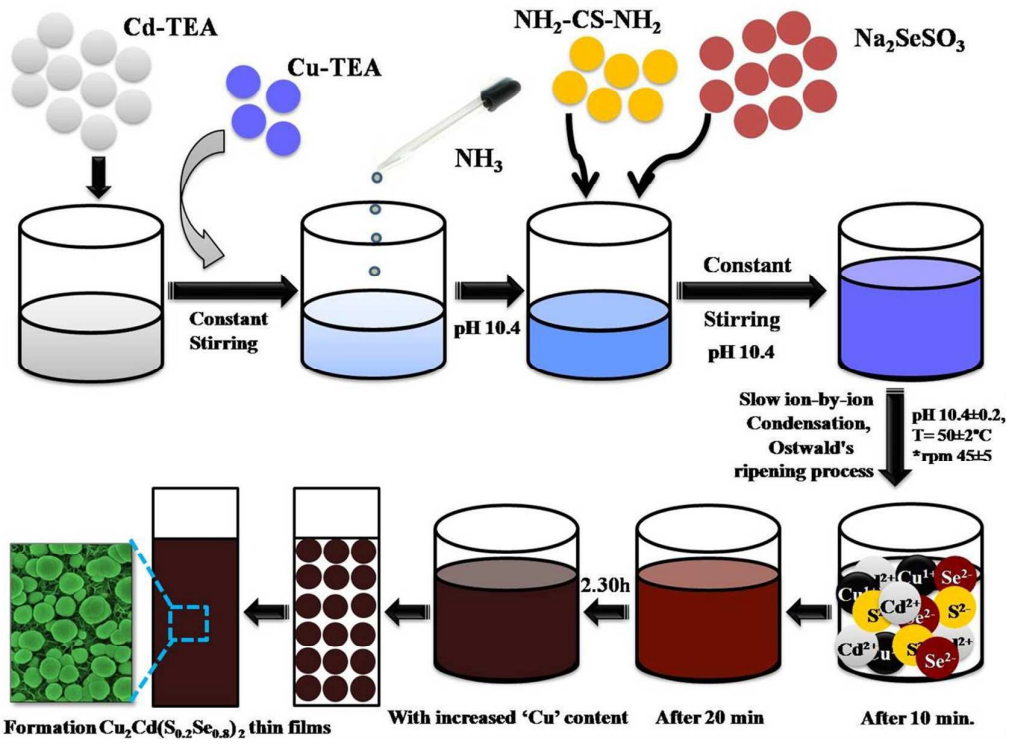


***Fig. 2*** *Schematic growth mechanism and stepwise experimental pathway for the synthesis of quaternary thin films.*

Later, all ions are starting to release slowly from the dissociation of the respective precursor complex. Such slow release of ions and formation of void free thin films is possible through the APT method as compared to the sophisticated and routine aqueous chemical techniques. Overall growth mechanism for thin film formation via APT is schematically demonstrated in Fig. 2.

### 3.2 Thickness measurement

The thickness of ternary ($C_0$) and quaternary ($C_1$ to $C_4$) thin films is found in a range of 815 nm to 930 nm. The thickness of all thin films is tabulated in Table 2.

### 3.3 Optical absorption study

Fig. 3(a) indicates optical absorption spectra of thin films in the 350 nm to 1150 nm wavelength range. With increased Cu content light absorption edge shifted to a higher wavelength range, which is clearly seen from Fig. 3(a).

New Journal of Chemistry Accepted Manuscript

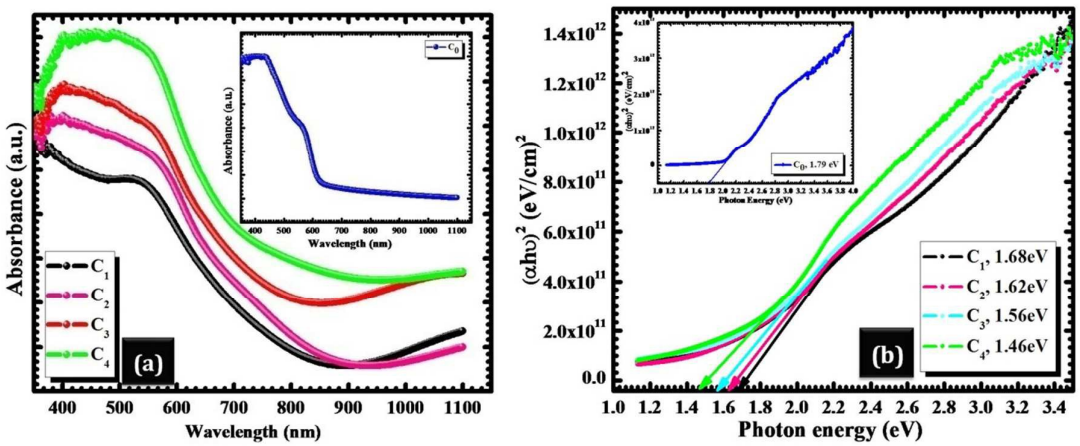


***Fig. 3(a)*** *Optical absorption spectra of $C_1$ to $C_4$ thin films, Inset: optical absorption spectrum of $C_0$ thin film and* ***(b)*** *plots of $(ahv)^2$ vs the photon energy ($hv$) of $C_1$ to $C_4$ thin films, Inset: plots of $(ahv)^2$ vs. photon energy ($hv$) of $C_0$ thin film.*

The shifting of absorption edge to the higher wavelength range is the indicative of effective deposition and increase in film thickness correspondingly. Generally, thicker films having well grown large crystal, which absorbs large amounts of photon energy [27]. The optical band gap energy values have been determined using the Tauc plot as shown in Fig. 3(b). The optical band gap energy was obtained by extrapolating straight line portion of the graph $(\alpha h\nu)^2$ *vs* photon energy ($h\nu$) at $\alpha$=0 to energy axis.

***Table 2*** *Statistics of thickness, optical band gap (Eg), crystallite size (D), dislocation density (δ) and micro-strain (ε).*

| Sample Code | Thickness (nm) | Band Gap ($E_g$) (eV) | Crystallite Size (D) (nm) | Dislocation Density (δ) $10^{-4}$ (lines $m^{-2}$) | Micro strain (ε) $10^{-4}$ (lines$^{-2}$ $m^{-4}$) |
|---|---|---|---|---|---|
| **$C_0$** | 815 | 1.79 | 79 | 1.60 | 4.50 |
| **$C_1$** | 859 | 1.68 | 56 | 3.18 | 6.61 |
| **$C_2$** | 890 | 1.62 | 61 | 2.68 | 6.22 |
| **$C_3$** | 909 | 1.56 | 64 | 2.44 | 5.98 |
| **$C_4$** | 930 | 1.46 | 65 | 2.36 | 5.90 |

New Journal of Chemistry Accepted Manuscript

Obtained optical band gap energy was found in the range of 1.68 eV to 1.46 eV for Cu containing thin films ($C_1$-$C_4$) and that of without Cu content thin film ($C_0$) shows the band gap at 1.79 eV (Table 2). The ternary and quaternary thin films show the absorption coefficient at $10^6$ $cm^{-1}$. The decrease in optical band gap energy is might be due to the formation of thicker and well defined grain with increase the Cu content in the ternary system. The linear nature of absorption plots indicates direct allowed type of transition.

### 3.4 Structural study

The phase formation and crystal structure were confirmed using X-ray diffraction (XRD) patterns in 2θ range of 20° to 70°. Fig. 4 (a,b) shows the XRD pattern of ternary ($C_0$) and QMMC ($C_1$ to $C_4$) thin films. All XRD patterns indicate intense diffraction peaks confirming the formation of nanocrystalline thin films [25]. The ternary thin film has major intense peaks at (100), (002), (101), (102), (110), (103) with respective (*hkl*) planes, which is in good agreement with the standard *JCPDS* data (49-1459) [12]. So, sample $C_0$ shows the formation of thin films through pure phase hexagonal crystal structure. Further, XRD spectra of QMMC thin films show peaks of Cd(SSe), $Cu_2S$, $Cu_2Se$ phases. Observed (100), (002), (101), (102), (110), (103) planes correspond to the Cd(SSe) phase (*JCPDS* Card No. 49-1459), (101), (102), (103), (202) planes for $Cu_2S$ phase (*JCPDS* Card No. 84-0206), while (200), (220), (311), (400) planes for $Cu_2Se$ phase (*JCPDS* Card No. 75-0889). There are no *JCPDS* data available for synthesized QMMC thin films. Hence, the obtained peaks position is considered by comparing peak positions with Cd(SSe), $Cu_2S$ and $Cu_2Se$ which are given in standard *JCPDS* data cards (49-1459), (84-0206) and (75-0889) respectively. The XRD patterns reveal that quaternary thin films possess mixed hexagonal and cubic crystal structures.

Careful observation of XRD patterns ($C_1$ to $C_4$) indicates that some major dominant peaks remain unchanged and some new peaks appear with increased copper content in the ternary system. Additional new peaks in the XRD pattern (Fig. 4(b)) indicate formation of new phases in QMMC thin films due to the copper content [28]. Such a successive increase in intensities of diffraction peaks is attributed to the incorporation of Cu in the crystal lattices of Cd(SSe), the nanosized thin film formation and good crystalline nature. Also, the ionic radius of $Cu^+$ (0.91 Å) is smaller than the



New Journal of Chemistry Accepted Manuscript

ionic radius of $Cd^{2+}$ ion (1.09 Å), suggesting that $Cu^{+}$ ions were successfully incorporated into the lattice of QMMC thin films.

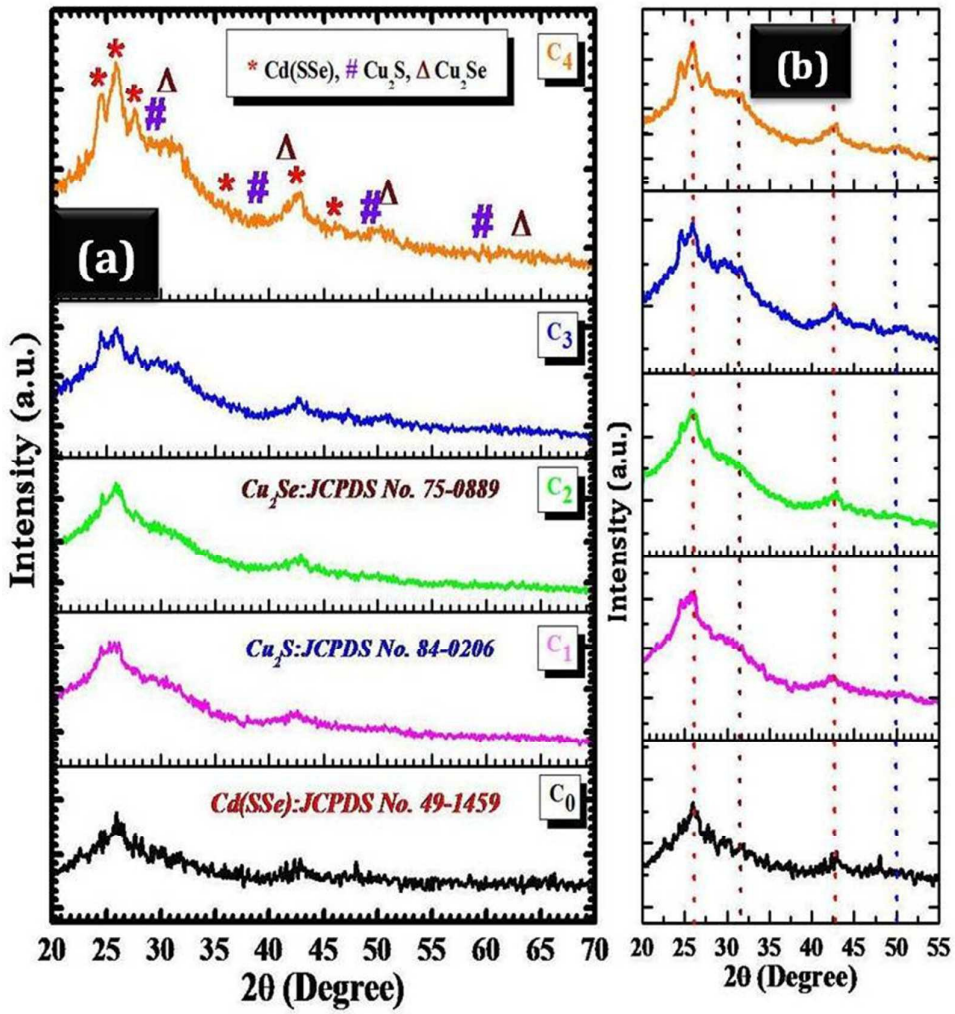


***Fig. 4 (a)*** *XRD patterns of ternary and quaternary thin films and* ***(b)*** *The magnified region of quaternary ($C_1$ to $C_4$) thin films peaks (2θ= 20° to 55°).*

Calculated interplanner *'d'* values are compared with standard values of Cd(SSe), $Cu_2S$, $Cu_2Se$ and are given in Table. 2. The last column of Table 3 shows the difference between calculated and the standard *'d'* values. The crystallite size (D) is calculated by using well known Scherrer formula [12]. Crystallite size of $C_0$, $C_1$, $C_2$, $C_3$ and $C_4$ thin films varied from 79, 56, 61, 64 and 65 nm respectively. This improvement in crystallite size with minimum interfacial energy is beneficial for effective light absorption. From calculated crystallite size (D), dislocation density (δ) and micro strain (ε) for all thin films were calculated using well known equations [12]. The calculated δ and ε indicates



New Journal of Chemistry Accepted Manuscript

that values are decreasing with the increase in Cu-content in QMMC thin films (Table 2). The decrease in δ and ε attributed to lower defect level, grain boundary and improvement in crystallite size of QMMC thin films [27, 28]. So, formation of high quality thin films occurs through a decrease in lattice imperfection [29-31].

The overall XRD study demonstrates the with increase in the Cu-content formation of mixed phases are observed with crystalline in nature. But, as per our literature survey based on other quaternary materials obtained XRD patterns does not show highly intense diffraction peaks. This is may be due to the low temperature synthesis and used without post treatments such as vacuum annealing at different atmosphere, rapid thermal annealing in presence of S or Se source.

***Table 3*** *The XRD parameters of synthesized thin films.*

| **Phase** | **2θ** | ***(hkl)*** | **d(Å)$_{Exp.}$** | **d(Å)$_{JCPDS.}$** | **Δd(Å) = d(Å)$_{Exp}$ - d(Å)$_{JCPDS.}$** |
|---|---|---|---|---|---|
| **Cd(SSe) [49-1459]** | 24.50 | (100) | 3.6290 | 3.6067 | 0.0223 |
| | 26.02 | (002) | 3.4203 | 3.3890 | 0.0313 |
| | 27.68 | (101) | 3.2189 | 3.1850 | 0.0339 |
| | 36.15 | (102) | 2.4824 | 2.4700 | 0.0124 |
| | 42.65 | (110) | 2.1178 | 2.0880 | 0.0298 |
| | 46.13 | (103) | 1.9658 | 1.9210 | 0.0448 |
| **$Cu_2S$ [84-0206]** | 29.04 | (101) | 3.0711 | 3.0600 | 0.0111 |
| | 38.87 | (102) | 2.3147 | 2.4113 | 0.0966 |
| | 49.15 | (103) | 1.8518 | 1.8877 | 0.0359 |
| | 59.73 | (202) | 1.5465 | 1.5300 | 0.0165 |
| **$Cu_2Se$ [75-0889]** | 29.64 | (200) | 3.0063 | 2.9200 | 0.0863 |
| | 41.59 | (220) | 2.1693 | 2.0647 | 0.1046 |
| | 51.42 | (311) | 1.7749 | 1.7608 | 0.0141 |
| | 63.83 | (400) | 1.4695 | 1.4600 | 0.0095 |

New Journal of Chemistry Accepted Manuscript

### 3.5 Morphological study

Fig. 5 shows FESEM micrographs of synthesized thin films. FESEM images clearly indicate that formation of uniform, pinhole free with well adherent thin films. Fig. 5(a,b) show FESEM micrographs of ternary thin film ($C_0$). The aggregated bunch of nanosphere like morphology was formed by smaller nanospheres, which is clearly seen in FESEM images of Fig. 5(a,b). Fig. 5(c,d) demonstrates the low and high magnification FESEM images of QMMC thin film ($C_1$). The low magnification FESEM image indicates the transformation of an aggregated bunch of nanospheres like morphology into the erratically orientated nanostructured network surface morphology after addition of copper and formation of QMMC thin films. Also, these contain a smaller number of spheres, which are interlinked and merged into erratically grown network (Fig. 5(c,d)). Fig. 5(e,f) are the FESEM images of sample $C_2$ at low and high magnification respectively. Fig. 5(e) reveals the formation of the merged surface morphology of erratically orientated nanostructured network and spherically grown morphology. The high magnification FESEM image shown in Fig. 5(f) indicates merged morphology containing spheres were grown comparatively larger size than the previous sample. It means that with increased Cu content in QMMC thin films aggregation of nanostructured networks with increase in number and size of spherically grown morphology was observed. The FESEM images of sample $C_3$ are shown in Fig. 5(g,h). The low magnification FESEM image of Fig. 5(g) illustrates the increased compactness in nanostructured network morphology with an increase in the number of spherically grown morphology. The high magnification FESEM image (Fig. 5(h)) indicates spherically grown morphology formed by more compact and tightly interconnected smaller nanospheres compared to sample $C_2$. Fig. 5(i,j) show FESEM images of sample $C_4$. As compared to other samples ($C_1$, $C_2$, $C_3$) the FESEM images of sample $C_4$ clearly indicates more compactness and larger growth of spherically grown morphology with networked surfaces. The overall observation of FESEM study concludes that the mixed and merged surface morphology is formed with increased in Cu content in the QMMC thin films [32].

New Journal of Chemistry Accepted Manuscript

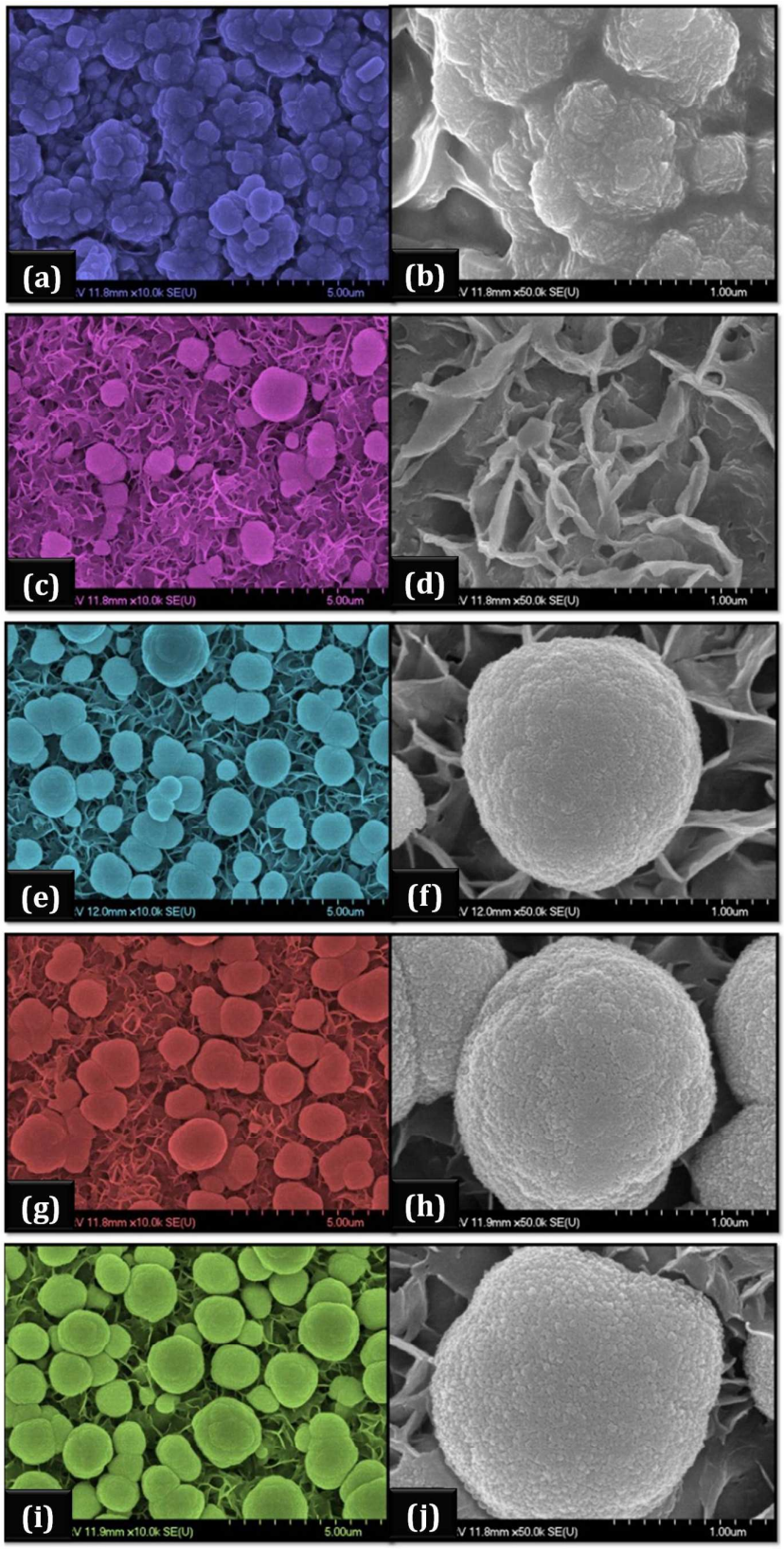


***Fig. 5*** *FESEM micrographs of* ***(a, b)*** $C_0$, ***(c, d)*** $C_1$, ***(e, f)*** $C_2$, ***(g, h)*** $C_3$ *and* ***(i, j)*** $C_4$ *thin films.*

New Journal of Chemistry Accepted Manuscript

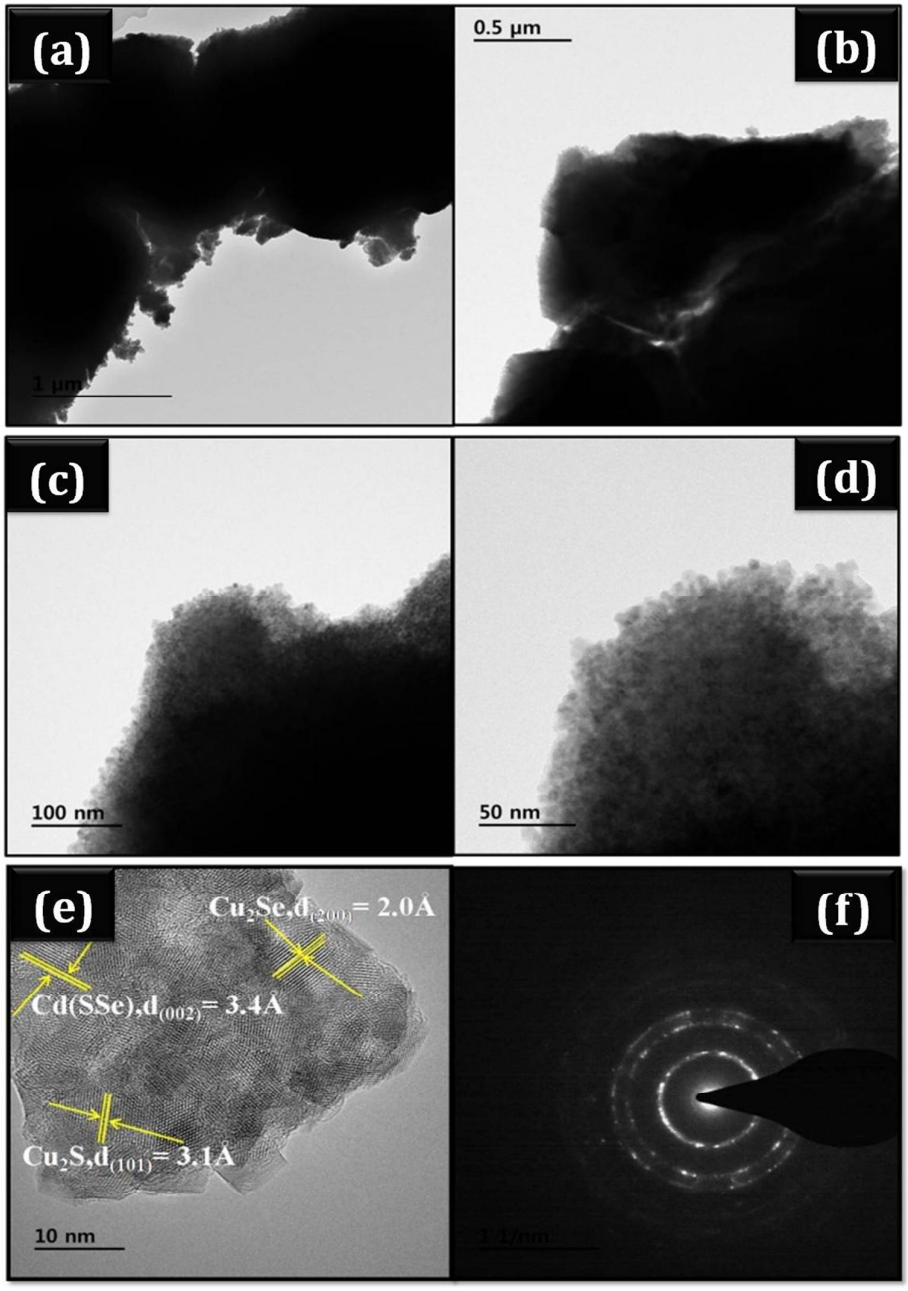


***Fig. 6 (a-e)*** *HRTEM images and* ***(f)*** *SAED pattern of $C_4$ thin film.*

The analysis of QMMC sample ($C_4$) was further characterized using HRTEM and SAED pattern at different magnifications for detail information about particles growth and surface modifications. Fig. 6 highlights HRTEM images and SAED pattern of QMMC thin film ($C_4$).Fig. 6(a,b) images show the formation of compact and well interconnected nanoparticles. Also, such well grown nanoparticles arranged void free manner, which is in good agreement with FESEM results. Fig. 6(c,d) shows HRTEM images, which reveals



New Journal of Chemistry Accepted Manuscript

that formed nanostructured surface morphology has covered overall substrate surface. Fig. 6(e) indicates the good crystalline nature of thin film with lattice fringes of $d_{(002)}$= 3.4 Å for Cd(SSe), $d_{(101)}$= 3.1 Å for $Cu_2S$ and $d_{(200)}$= 2.0 Å for $Cu_2Se$. These lattice fringes are well consistent with obtained XRD results. Further, the SAED pattern (Fig. 6(f)) shows the formation of distinct ring pattern. Such a bright, distinct ring pattern confirms nanocrystalline nature of synthesized materials [33]. From above discussion, it clearly demonstrated that deposited QMMC thin films by the APT method were of nanocrystalline nature. While, obtained SAED pattern results are good accordance with the XRD as well as FESEM data.

### 3.6 Compositional analysis

EDS spectrums of ternary ($C_0$) and representative quaternary ($C_4$) thin films are given in Fig. 7(a,b) respectively. Fig. 7(a) show that peaks at 3.13, 2.50 and 1.38 keV confirms the presence of $Cd^{2+}$, $S^{2-}$ and $Se^{2-}$ elements ($C_0$) respectively. Fig. 7(b) shows the peaks at 0.93, 3.13, 2.50 and 1.38 keV for $Cu^{+}$, $Cd^{2+}$, $S^{2-}$ and $Se^{2-}$ elements ($C_4$) respectively. EDS study clearly confirmed that the presence of Cd, S, Se elements in the ternary and Cu, Cd, S, Se elements in the quaternary synthesized thin films respectively. Fig. 8(a) demonstrates the XPS survey spectrum of the representative $C_4$ sample. The survey spectrum shows the presence of Cu, Cd, S, Se, C and O elements. Presence of O may be due to extrinsic contaminations, such as adsorption of $CO_2$, $O_2$ and $H_2O$ on the film surface from the atmosphere [16, 34]. Binding energies obtained in the XPS analysis were standardized for specimen charging by using C1s as a reference at 285.02 eV. The high resolution core level XPS spectrum of Cu2p is shown in Fig. 8(b). The Cu2p core level XPS spectrum shows two narrow and asymmetric peaks for $Cu2p_{1/2}$ and $Cu2p_{3/2}$ at 952.01 eV and 932.18 eV binding energies respectively.

New Journal of Chemistry Accepted Manuscript

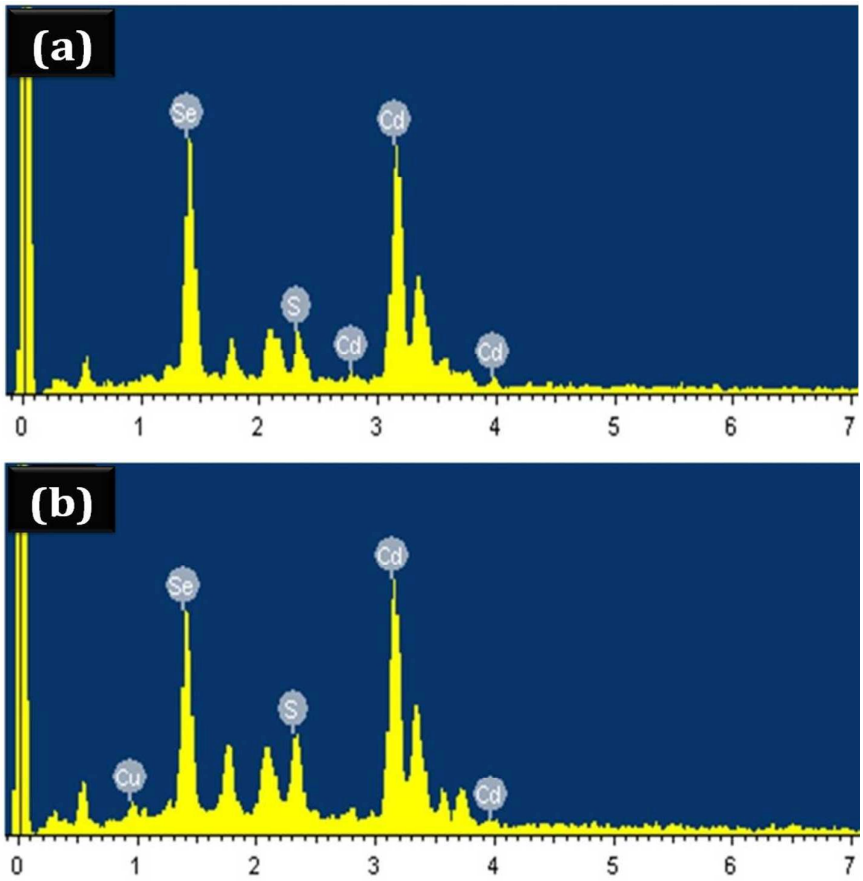


***Fig. 7*** *EDS spectrum of* ***(a)*** $C_0$ *and* ***(b)*** *representative* $C_4$ *thin film.*

The presence two distinct peaks with splitting energy at 19.83 eV confirm that Cu was in +1 oxidation states [35, 36]. From the spin-orbital coupling interaction in Cd3d two distinct core level peaks were separated as $Cd3d_{5/2}$ at a binding energy of 404.97 eV and $Cd3d_{3/2}$ at a binding energy of 411.68 eV (Fig. 8(c)). The high resolution core level XPS spectrum of S2p of Fig. 8(d) indicates single peak for S2p located at 159.96 eV binding energy, which is well consistent with range expected for the S in sulfide phase [36]. The core level XPS spectrum of Se3d (Fig. 8(e)) shows a peak at 54.07 eV, which is in good agreement with values reported for Se (-II) phase and metal bonded Se [37]. The observed binding energies for all elements are in their respective oxidation state confirms $Cu^{+}$, $Cd^{2+}$, $S^{2-}$ and $Se^{2-}$ ions were present in deposited thin film ($C_4$).



New Journal of Chemistry Accepted Manuscript

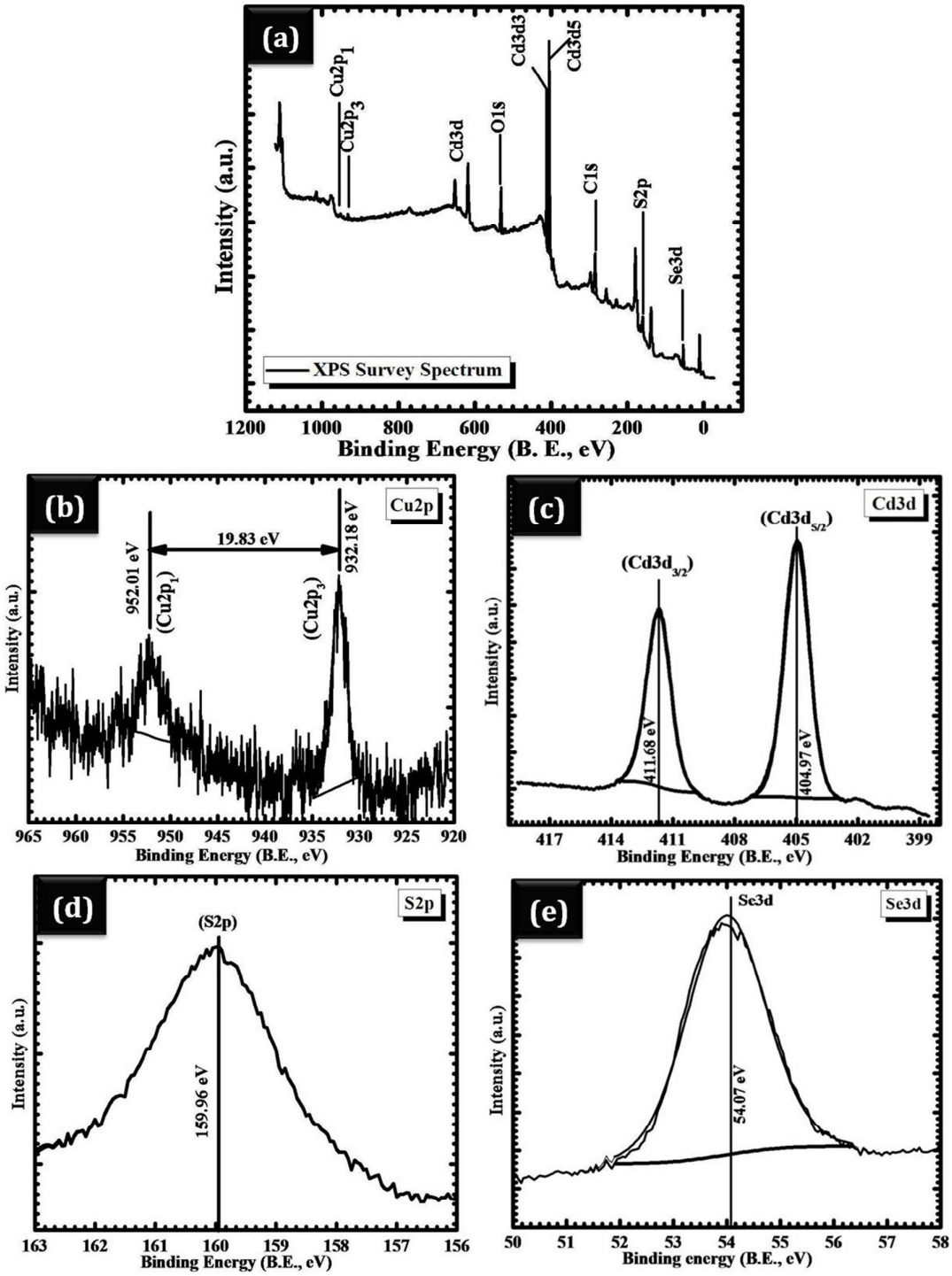


***Fig. 8 (a)*** *XPS survey spectrum of $C_4$ thin film,* ***(b)*** *high resolution core level XPS spectrum of Cu,* ***(c)*** *high resolution core level XPS spectrum of Cd,* ***(d)*** *high resolution core level XPS spectrum of S and* ***(e)*** *high resolution core level XPS spectrum of Se.*

New Journal of Chemistry Accepted Manuscript

### 3.7 Electrical conductivity and thermoelectric power measurement study

Fig. 9 (a) shows EC plots of lnσ *vs* 1000/T for QMMC thin films ($C_1$, $C_2$, $C_3$ and $C_4$) and inset show plot of the ternary thin film ($C_0$).

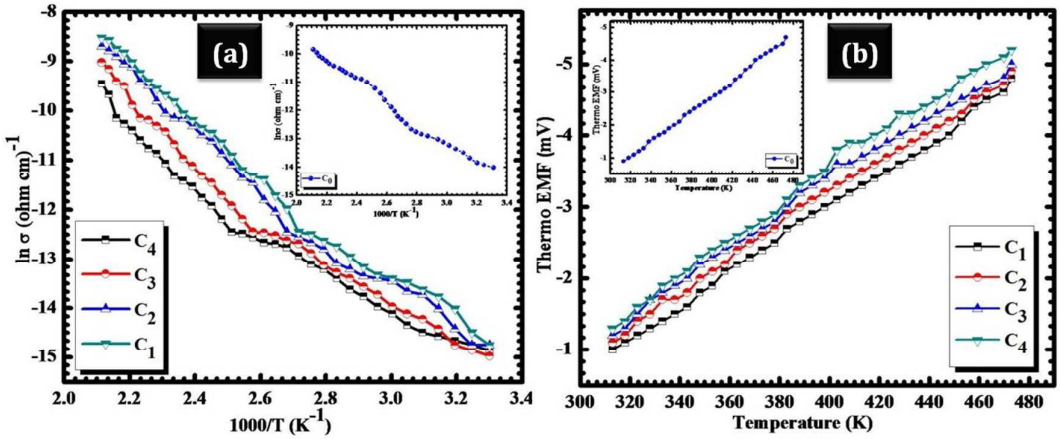


***Fig. 9 (a)*** *Plots of lnσ vs. 1000/T of $C_1$- $C_4$ thin films, Inset: plot of lnσ vs. 1000/T of $C_0$ thin film and* ***(b)*** *plots of thermo EMF vs. Temperature of the $C_1$- $C_4$ thin films, Inset: plot of thermo EMF vs. Temperature of $C_0$ thin film.*

From this plots, it was observed that conductivity increases with the increase in temperature assigning semiconducting nature [38, 39]. Further activation energy was calculated from known equation [40]. The activation energy values are tabulated in Table 4. The decrease in activation energy illustrates the semiconducting behavior of thin films [40, 41].

***Table 4*** *Electrical parameters of synthesized thin films.*

| Sample Code | Activation Energy ($E_a$, $10^{-3}$, eV) | Carrier Concentration ($n$, $10^{19}$ cm$^{-3}$) | Mobility ($\mu$, $10^{-7}$, cm$^{-2}$V$^{-1}$ S$^{-1}$) |
|---|---|---|---|
| $C_0$ | 0.045 | 3.533 | 4.552 |
| $C_1$ | 0.096 | 3.387 | 5.131 |
| $C_2$ | 0.093 | 3.568 | 5.012 |
| $C_3$ | 0.081 | 3.595 | 3.172 |
| $C_4$ | 0.078 | 3.614 | 3.167 |

New Journal of Chemistry Accepted Manuscript

Fig. 9(b) shows plots of thermo EMF vs. Temperature of the QMMC thin films ($C_1$, $C_2$, $C_3$ and $C_4$) and inset shows a plot of thermo EMF vs. Temperature of the ternary thin film ($C_0$). The negative polarity of generated thermo *emf* indicates thin films have *n*-type semiconducting nature. From TEP plots of carrier concentration ($n$) and mobility ($\mu$) were calculated [38] and calculated data of $n$ and $\mu$ summarized in Table 4. The $n$ increase and $\mu$ decrease for ternary as well as QMMC thin films (Table 4) might be due to the decrease in antistructural defects [40, 41].

### 3.8 Photoelectrochemical property

Fig. 10 illustrates the *J-V* curves of all thin films studied in order to assess their PEC performance. Table 4 indicates tabulated values of solar cell parameters extracted from *J-V* curves. PEC cells were formed by deposited thin films as working electrodes and graphite rod as a counter electrode. PEC cell parameters such as fill factor (FF), conversion efficiency ($\eta$), values of series resistance ($R_s$) and shunt resistance ($R_{sh}$) of all samples were calculated from well known equations [12]. All values are summarized in Table 5. The PEC performance of all samples was conceded by forming following cell configuration,

$$\textit{Glass-ITO/ } Cu_2Cd(SSe)_2\textit{/ } (Na_2S\text{-}NaOH\text{-}S)_{aq.}\textit{/G}$$

From *J-V* measurements, values of $J_{sc}$ for $C_0$, $C_1$, $C_2$, $C_3$ and $C_4$ thin films were found to be 0.630, 1.029, 1.044, 1.046 and 1.235 mA/cm$^2$ and that of corresponding values of $V_{oc}$ were found to be 810, 450, 452, 455 and 437 mV respectively. From Table 5 it was observed that initially QMMC chalcogenides thin film ($C_1$) shows the low conversion efficiency as compared to the ternary sample ($C_0$). But as Cu content increased effective power conversion efficiency was found to be enhanced. The morphological study clearly pointed out that the aggregated bunch of nanospheres like morphology of the ternary sample ($C_0$) has a comparatively large surface for light absorption. While, that of sample $C_1$ illustrates erratically orientated nanostructured networked surface morphology. Such morphology is having a low surface area for light absorption, which results in lower conversion efficiency. Further sample $C_2$ contains merged surface morphology of erratically orientated nanostructured network and spherically grown morphology.



New Journal of Chemistry Accepted Manuscript

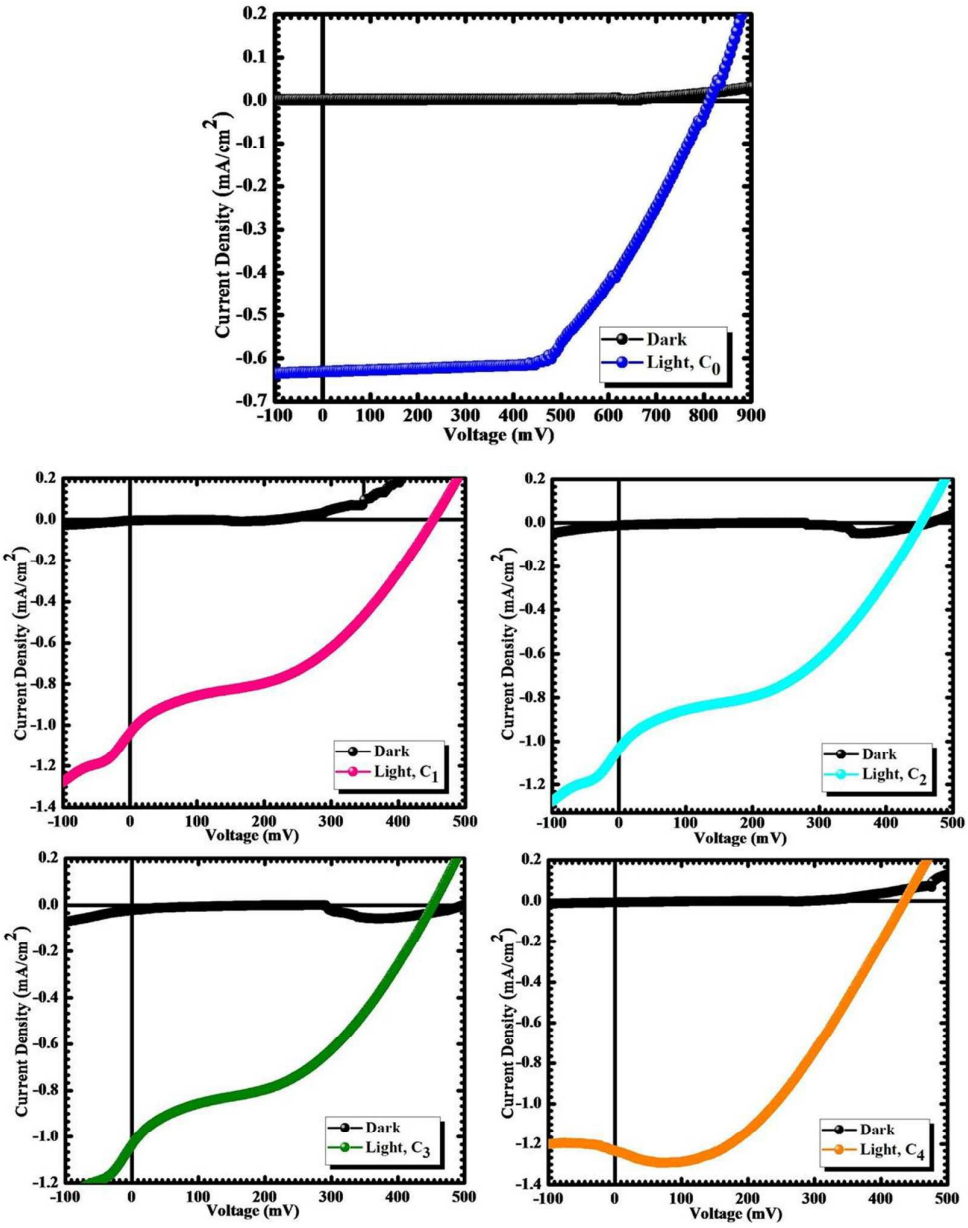


***Fig. 10*** *J–V characteristic curves of the $C_0$- $C_4$ thin films.*

This merged surface morphology having an increased surface area due to the formation of spherically grown nanostructures and effective scattering through nanonetworked porous surface morphology. Further sample $C_3$ and $C_4$ have better conversion efficiency due to more compactness and larger growth of spherically grown morphology with networked surfaces [41]. In addition to this, the thickness of synthesized thin films is increasing with the increase in Cu-content. Such increase in film thickness is beneficial for solar cell application, because thicker films have well



New Journal of Chemistry Accepted Manuscript

grown atoms having a large surface area and favorable for absorption of light radiations [16]. Such improvement in surface area is highly suitable for PEC cell application. In the present investigation the improvement in conversion efficiency is correlated with the increase in film thickness as well as the formation of hierarchical microstructures of quaternary thin films [16].

***Table 5*** *J-V parameters of synthesized thin films.*

| Sample Code | $J_{sc}$ (mA/cm²) | $V_{oc}$ (mV) | $J_{max}$ (mA/cm²) | $V_{max}$ (mV) | $R_s$ (Ω) | $R_{sh}$ (Ω) | FF | $\eta$ (%) |
|---|---|---|---|---|---|---|---|---|
| $C_0$ | 0.630 | 810 | 0.544 | 554 | 343 | 6221 | 0.60 | 1.02 |
| $C_1$ | 1.029 | 450 | 0.713 | 263 | 195 | 2286 | 0.39 | 0.61 |
| $C_2$ | 1.044 | 452 | 0.720 | 264 | 192 | 1876 | 0.40 | 0.62 |
| $C_3$ | 1.046 | 455 | 0.725 | 276 | 187 | 1751 | 0.41 | 0.66 |
| **$C_4$** | **1.235** | **437** | **0.916** | **258** | **172** | **1650** | **0.43** | **0.77** |

Such morphology is formed by smaller nanospheres to form a well grown spherical morphology, which are having a large surface area for effective light absorption as like 'light trapping' phenomena. That of erratically orientated nanostructured network morphology has a better pathway of electron flow based on 'light scattering' phenomenon [16] (as shown schematically in Fig. 11).

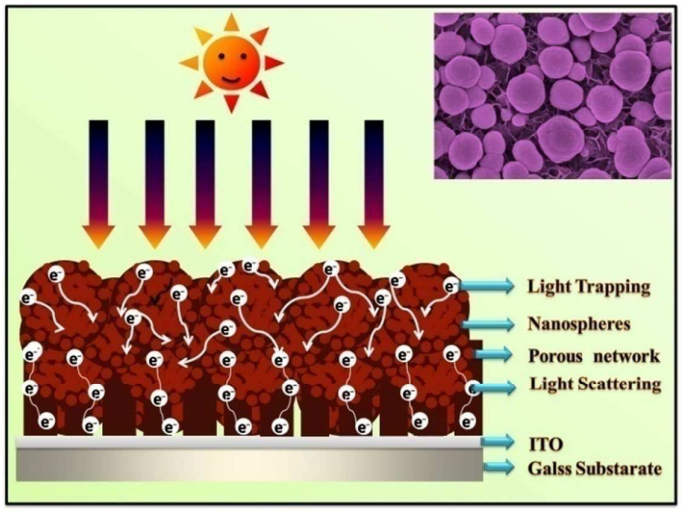


***Fig. 11*** *Schematic representation of light absorption mechanism through synthesized thin films.*



New Journal of Chemistry Accepted Manuscript

## 4 Conclusions

Quaternary mixed metal chalcogenide thin films were synthesized by using the arrested precipitation technique. The synthesized thin films show enhancement in photocurrent with an increase in Copper-content. Such improvement in conversion efficiency is quite comparable with other well known quaternary materials synthesized by sophisticated physical techniques. The optostructural study showed that synthesized quaternary thin films have mixed phase crystal structure and band gap energy in the range of 1.79 eV to 1.46 eV. Morphological study clearly indicated that hierarchical microstructures are developed with nanocrystalline nature. Compositional analysis confirms synthesized thin films are in requisite composition. The electrical conductivity study illustrated *n*-type semiconducting nature of thin films. The *J-V* curves demonstrated that QMMC thin films showed the improvement in conversion efficiency with increased Copper-content.

## Acknowledgement

One of the authors, Mr. Kishorkumar V. Khot is very much thankful to Department of Science and Technology (DST), New Delhi for providing DST-INSPIRE fellowship for financial support (Registration No. IF130751). This research was supported by the Basic Science Research Program through the National Research Foundation of Korea (NRF) funded by the Ministry of Education (NRF-2009-0094055).

## References

1) J. Zhao, J. Zhang, W. Wang, P. Wang, F. Li, D. Ren, H. Si, X. Sun, F. Ji, Y. Hao, *Dalton Trans*., 2014, **43**,16588.
2) X. Hu, Q. Zhang, X. Huang, D. Li, Y. Luo and Q. Meng, *J. Mater. Chem.,* 2011, **21**, 5903.
3) M. Y. Chiang, S. H. Chang, C. Y. Chen, F. W. Yuan, H. Y. Tuan*, J. Phys. Chem. C,* 2011,**115**, 1592.
4) D. Aldakov, A. Lefrançois, P. Reiss, *J. Mater. Chem. C,* 2013, **1**, 3756.
5) S. Lakehal, S. Achour, C. Ferrari, E. Buffani, F. Rossi, F. Fabrri, *Superlattice Microst.*, 2014, **72**, 253.
6) T. Hong, Z. Liu, W. Yan, B. Wang, X. Zhang, J. Liu, J. Wang, J. Han, *Chem. Commun.,* 2015, **51**, 13678.
7) K. Guo, Z. Liu, J. Han, X. Zhang, Y. Li, T. Hong, C. Zhou, *J. Power Sources,* 2015, **285**, 185.



New Journal of Chemistry Accepted Manuscript

8) Z. Liu, Y. Wang, B. Wang, Y. Li, Z. Liu, J. Han, K. Guo, Y. Li, T. Cui, L. Han, C. Liu, G. Li, *Int J Hydrogen Energ,* 2013, **38**, 10226.

9) S. S. Mali, P. S. Patil, and C. K. Hong, *ACS Appl. Mater. Interfaces*, 2014, **6**, 1688−1696.

10) S. Siebentritt, L. Gütay, D. Regesch, Y. Aida, V. Deprédurand, *Sol. Energ. Mat. Sol. C.,* 2013, **119**, 18.

11) T. Klinkert, T. Hildebrandt, M. Jubault, F. Donsanti, J. François G. N. Naghav, *Thin Solid Films*, doi.org/10.1016/j.tsf.2014.09.074.

12) K. V. Khot, S. S. Mali, N. B. Pawar, R. R. Kharade, R. M. Mane, V. V. Kondalkar, P. B. Patil, P. S. Patil, C. Hong, J. H. Kim, J. Heo and P. N. Bhosale, *New J. Chem,* 2014, **38**, 5964.

13) A. A. Yadav, E. U. Masumdar, *J. Alloys Compd.,* 2010, **505**, 787.

14) D. O. Dumcenco, Y. M. Chen, Y. S. Huang, F. Firszt, S. Egowski, H. Eczynska, A. Marasek, K. K. Tiong, *J. Alloys Compd.*, 2010, **491**, 472.

15) M. M. Salunkhe, N. B. Pawar, K. V. Khot, P. S. Patil, T. M. Bhave, P. N. Bhosale, *J Mater Sci: Mater Electron*, 2015, **26**, 2921.

16) K. V. Khot, S. S. Mali, R. R. Kharade, R. M. Mane, P. S. Patil, C. K. Hong, J. H. Kim, J. Heo, P. N. Bhosale, *J Mater Sci: Mater Electron*, 2014, **25**, 5606.

17) S. D. Chavhan, R. S. Mane, T. Ganesh, L. Wonjoo, S. H. Han, S. Senthilarasu, S. H. Lee, *J. Alloys Compd*., 2009, **474**, 210.

18) J. B. Chaudhari, N. G. Deshpande, Y. G. Gudage, A. Ghosh, V. B. Huse, R. Sharma, *Appl. Surf. Sci.,* 2008, **254**, 6810.

19) F. Liu, Y. Lai, J. Liu, B. Wang, S. Kuang, Z. Zhang, J. Li, Y. Liu, *J. Alloys Compd.* 2010, **493,** 305.

20) J. Yuan, C. Shao, L. Zheng, M. Fan, H. Lu, C. Hao, D. Tao, *Vacuum*., 2014, **99**, 196-203.

21) R. C. Valderrama, P. J. Sebastian, J. P. Enriquez, S. A. Gamboa, *Sol. Energ. Mat. Sol. C.,* 2005, **88**, 145.

22) H. Dong, A. Quintilla, M. Cemernjak, R. Popescu, D. Gerthsen, E. Ahlswede, C. Feldmann, *J Colloid Interf. Sci*., 2014, **415**, 103.

23) U. Dasgupta, S. K. Saha, A. J. Pal, *Sol. Energ. Mat. Sol. C.,* 2014, 12479.

24) Y. Kashiwaba, K. Isojima, K. Ohta, *Sol. Energ. Mat. Sol. C.,* 2003, **75**, 253.

25) S. D. Kharade, N. B. Pawar, Sawanta S. Mali, C. K. Hong, P. S. Patil, M. G. Gang, J. H. Kim, P. N. Bhosale, *J Mater Sci*, 2013, **48**, 7300.



New Journal of Chemistry Accepted Manuscript

26) S. Spiering, S. Paetel, F. Kessler, M. Igalson, H. A. Maksoud, *Thin Solid Films*, 2014, **11**, 27.

27) K. V. Khot, S. S. Mali, N. B. Pawar, R. M. Mane, V. V. Kondalkar, V. B. Ghanwat, P. S. Patil, C. K. Hong, J. H. Kim, J. Heo, P. N. Bhosale, *J. Mater. Sci.: Mater. Electron.,* 2014, **25**, 3762.

28) S. M. Patil, S. N. Gavale, R.K. Mane, N. S. Patil, S. S. Mali, P. S. Patil, P. N. Bhosale, *Arch. Phy. Res.,* 2012, **3 (3),** 245-257.

29) T. Kameyama, T. Osaki, K. Okazaki, T. Shibayama, A. Kudo, S. Kuwabatade, T. Torimoto, *J. Mater. Chem.,* 2010, **20**, 5319.

30) U. Pal, D. Samantha, S. Ghorai, A. K. Chaudhuri, *J. Appl. Phys.,* 1993**, 74**, 6368.

31) V. M. Garcia, M. T. S. Nair, P. K. Nair, R. A. Zingaro, *Semicond. Sci. Technol.,* 1997, **12,** 645.

32) S. S. Mali, C. A. Betty, P. N. Bhosale, P. S. Patil, C. K. Hong, *Sci. Rep.*, 2014, **4**, 5451.

33) N. B. Pawar, S. D. Kharade, S. S. Mali, R. M. Mane, C. K. Hong, P. S. Patil, P. N. Bhosale, *Solid State Sci,* 2014, **35**, 10-17.

34) S. S. Mali, C. A. Betty, P. N. Bhosale, P. S. Patil, *Electrochim. Acta,* 2012, **59,** 113.

35) G. Gordilloa, C. Calderon, P. Bartolo-Perez, *Appl Surf Sci.,* 2014, **305**, 506.

36) S. C. Riha, B. A. Parkinson, A. L. Prieto, *J. Am. Chem. Soc.* 2009, **131**, 12054.

37) T. Liu, Y. Hua, W. Chang, *Mat Sci Eng B,* 2014, **180**, 33.

38) S. H. Pawar, P. N. Bhosale, M. D. Uplane, S. Tamhankar, *Thin Solid Films*, 1983, **110,** 165-170.

39) S. H. Pawar, P. N. Bhosale, *Mater Chem Phys*, 1984, **11**, 461.

40) K. V. Khot, S. S. Mali, N. B. Pawar, R. R. Kharade, R. M. Mane, P. B. Patil, P. S. Patil, C. Hong, J. H. Kim, J. Heo and P. N. Bhosale, *RSC Adv.*, 2015, **5,** 40283.

41) M. M. Salunkhe, K. V. Khot, P. S. Patil, T. M. Bhave, P. N. Bhosale, *New J. Chem*, 2015, **39**, 3405.


New Journal of Chemistry Accepted Manuscript

# Photocurrent enhancement in $Cu_2Cd(SSe)_2$ photoanode synthesized via arrested precipitation route

**Kishorkumar V. Khot**[a], Sawanta S. Mali[b], Vishvanath B. Ghanwat[a], Suvarta D. Kharade[a], Rahul M. Mane[a], Chang Kook Hong[b], and Popatrao N. Bhosale[a*]

[a]*Materials Research Laboratory, Department of Chemistry, Shivaji University, Kolhapur-416004, India.*

[b]*Polymer Energy Materials Laboratory, Advanced Chemical Engineering Department, Chonnam National University, Gwangju, South Korea.*

[c]*Thin film Materials Laboratory, Department of Physics, Shivaji University, Kolhapur, India.*

*Corresponding Author E-mail address: p_n_bhosale@rediffmail.com*

*khotkishor75@gmail.com, Tel Number: 091-231-2609338.*

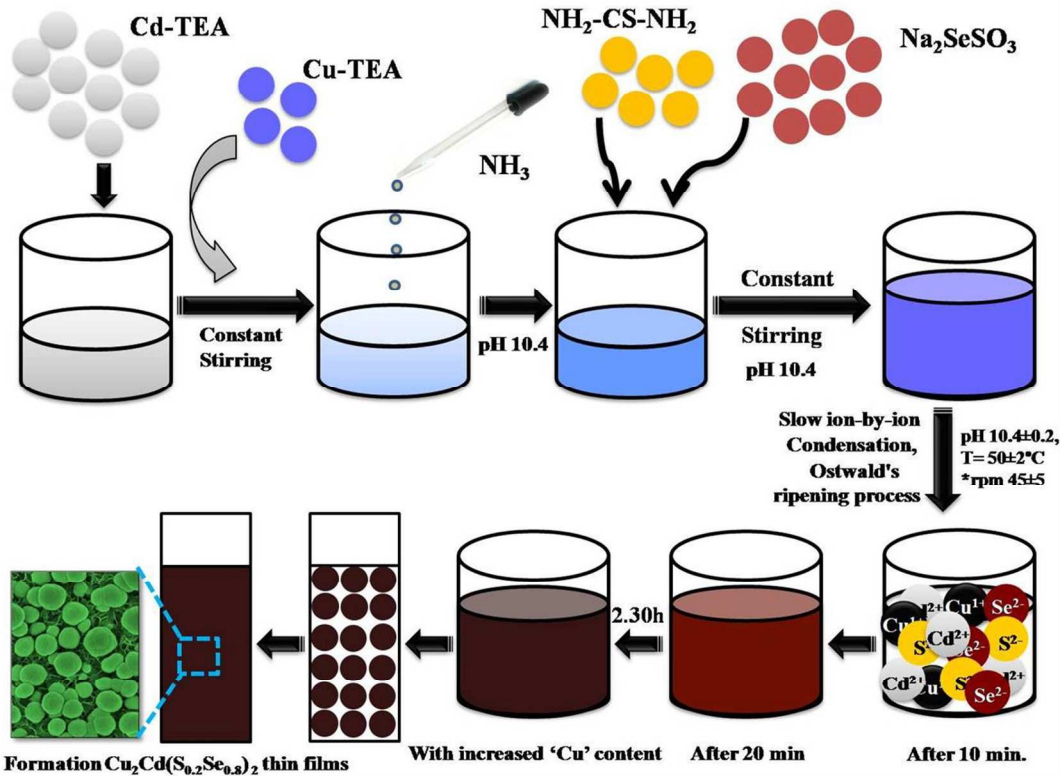


New Journal of Chemistry Accepted Manuscript